ISSN 2963-7511
Journal of Engineering Researcher and Lecturer, Vol. 4, No. 1, pp. 9-21, 2025

Performance analysis of inserted resonators in microstrip array antenna for biomedical applications

Cing Nuam Man[1*], Thanda Win[1], Hla Myo Tun[2], and Mya Mya Aye[1]

[1] Department of Electronic Engineering, Yangon Technological University, **Myanmar**
[2] Research Center, Yangon Technological University, **Myanmar**

*Corresponding Author: cnmanboih@gmail.com

Received: 06th January 2025; 1st Revised: 25th March 2025; 2nd Revised: 10th April 2025; Accepted: 15th April 2025

https://doi.org/10.58712/jerel.v4i1.177

Abstract: This paper investigates the use of inserted resonators in designing microstrip patch array antenna for biomedical applications, such as respiratory rate detection. The purpose of this study is to analyze size and placement of resonator, and slots which influence the overall performance. The antenna was constructed by connecting two single microstrip patch antennas (11.7mm × 15.7 mm×1.6 mm) on an FR4 substrate with a dielectric constant ($\varepsilon_r = 4.4$) to form (26 mm × 50mm × 1.6 mm). It achieves a miniaturized design of the expected resonance frequency with directional polarization, and provides good gain and bandwidth. The simulations were operated using FEKO software. The results and size of antenna were compared with references designs. The antenna was also designed for a 5-6 GHz frequency range, making it suitable for ISM band (Industrial, Medical, and Science) band range, low-power wireless applications, including Wi-Fi, and Bluetooth, as well as robotic systems, low-noise amplifier (LNA), 5 G applications, and WiFi 6E standard applications.

Keywords: microstrip patch array antenna; FR4 substrate; resonance frequency; resonator

1. Introduction

Monitoring devices for human vital signs are essential in assessing a person's general health and detecting events such as respiratory distress or heart attacks (Yang et al., 2018). Monitoring systems include both contact and noncontact monitoring devices that are used in various fields for different purposes. Contact monitoring devices are faced with the challenges of light weight, flexibility, low profile, and reliable communications (Liu et al., 2016). Noncontact monitoring devices measure parameters from a distance, often utilizing various sensors or technologies. In some cases, antennas are used as sensors for monitoring, such as in radar systems. Radar systems have been employed in a wide range of applications, including monitoring, remote sensing, ground penetrating radars, wall and through-wall imaging, surveillance, high data rate communication, and medical imaging. The ultra-wideband radar system operates by transmitting short-duration pulses and detecting the reflected pulses (Zito & Pepe, 2014). The pulses and echoes are radiated and received using antennas. The receiver antenna produces information, which is analyzed using appropriate signal processing techniques to evaluate the performance parameters of the microstrip patch antenna, such as SAR (Specific Absorption Rate), reflection coefficient (S1,1), radiation pattern, directivity, and polarization, all of which must be properly assessed (Kadir Al-Nahiun et al., 2021). Therefore, the antenna bandwidth must be sufficiently wide (a few gigahertz) to effectively transmit and receive the pulses (Zito & Pepe, 2014).

One of the specifications SAR, which is at different frequencies, was calculated numerically using the three-layer (Skin-Fat-Muscle) human body model (Poffelie et al., 2016). The relationship between the radar-reflected frequency and dielectric properties of the skin is based on how electromagnetic waves interact with biological tissues. When radar waves encounter the human body's skin, some of the energy is reflected and some is absorbed by the skin. The degrees of reflection and absorption depend on the frequency of the radar signal and the skin's

properties. In general, low-frequency radar waves (L-band or S-band) can penetrate deeper into the body before absorption of the clothing is far less than the reflection and absorption of the body. This is why the FSR (forward-scattering radar system) is insensitive to clothes (Yang et al., 2018). Furthermore, in most of the reflection-based bio-radars, respiration detection is performed by analyzing the micro-doppler signature changes caused by the slight movement of the chest wall (Yang et al., 2018). In biomedical applications, antenna design plays a crucial role in achieving optimal performance, where large bandwidth, appropriate resonance frequency, and high gain are essential for accurately capturing signals. To meet these requirements, the antenna design is analyzed by strategically placing slots and resonators in the patch.

Microstrip patch antennae are used for their advantages such as ease of fabrication (Poffelie et al., 2016), simple structure, low price, non-ionizing radiation, and ease of integration with microwave integrated circuits (Kadir Al-Nahiun et al., 2021; Lakrit et al., 2018; Liu et al., 2016; Pepe et al., 2013; Poffelie et al., 2016; Yang et al., 2018; Yousaf et al., 2021). There are several categories of microstrip patch antenna which can be cited some examples circular, square radiating element, triangular, and semicircular, but the most common is the rectangular element (Balanis, 2009). Therefore, in this paper, a C-band antenna with appropriate bandwidth (in GHz) is constructed using an inset-feed rectangular patch antenna for biomedical applications.

Specific information is crucial for biomedical applications, which require larger bandwidth and higher gain. A large bandwidth allows for the collection of more data, while a higher gain antenna improves signal strength. However, the main drawback of patch antennas is narrow bandwidth and low gain (Balanis, 2009; Lakrit et al., 2018). To achieve larger bandwidth and higher gain, several methods have been proposed, including the use of slots on the radiating element or ground plane, increasing substrate thickness, utilizing high permittivity substrates, modifying the basic planes, and array antenna (Hamad & Abdelaziz, 2019; Rojas et al., 2023). Patch antennas typically suffer from narrow bandwidth and low gain, limiting their effectiveness in high-performance applications (Balanis, 2009).

To address these challenges, various techniques, such as enhancing bandwidth and gain using the DGS (Defected Ground Structure) technique, have been developed (Emara et al., 2023), degrading the mutual coupling effect by adding a free space rectangular patch (Kumar et al., 2021), achieving wide bandwidth using the DGS method (Olawoye & Kumar, 2022). The introduction of slots on the radiating element or ground plane has been explored. The miniaturized design is also essential for a contactless breathing detection package. The antenna patch sizes (Alkurt et al., 2023; En-naghma et al., 2025; Natali et al., 2024; Raj & Mandal, 2024) are compared with this work. In this research work, the DGS (Defected Ground Structure), such as adding slots are at the ground side, and a resonator is added between the two antennas to improve the bandwidth and decrease the coupling effect. Additionally, the gain is enough for detecting the respiratory rate and the size of the antenna is more compact by adding the slots.

2. Material and methods

In this research work, the method adopted was design, analysis, and simulation. Defeating ground structure method using slots and resonators placement is analyzed and simulated. This work involves three steps: step 1 is the implementation of a single patch inset-feed microstrip antenna, step 2 is the array antenna to get higher gain, step 3 is the enhancement of gain using a resonator between patches, and step 4 is to enhance bandwidth using slots at the ground. The antenna uses a double-layer printed circuit board with a FR4 substrate.

2.1 Rectangular microstrip single patch antenna structure and design

There are four feeding techniques, which are microstrip line, coaxial prob, aperture coupling, and proximity coupling (Balanis, 2009). Rectangular microstrip patch antenna with inset-feed

technique is easy to design and offers good impedance matching and larger radiation efficiency compared to simple line transmission technique and coaxial feed technique (Balanis, 2009). Figure 1 is the flow of the research process.

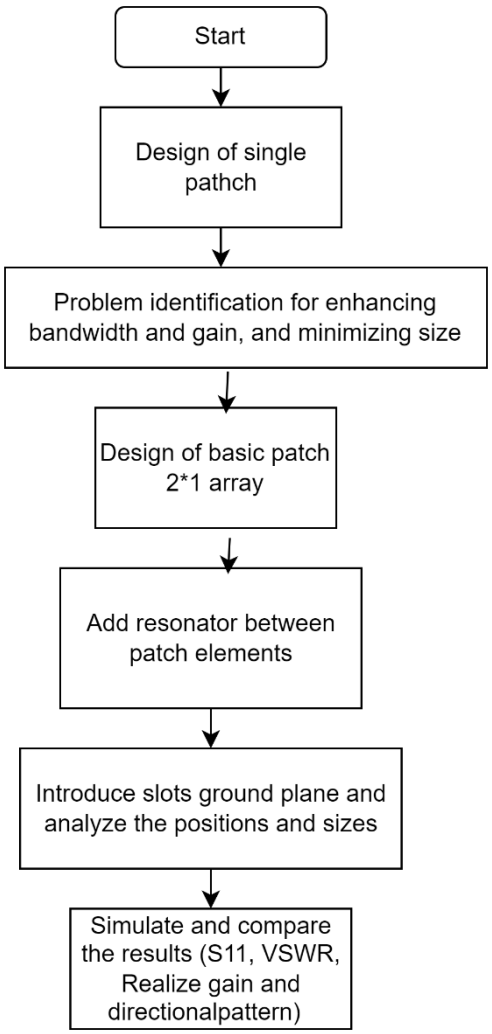

Figure 1. Flow of the research process

Figure 2 (a) illustrates the 3D patch symbol, and Figure .2 (b) shows the geometrical top view of the inset-feed along with the dimensions used in the simulation. Cut size (g) and depth of feed line (Y0) optimize the impedance matching, enhancing the antenna's performance. These parameters define the antenna's structural design. In the next section, the formulas used to calculate the dimensions are presented.

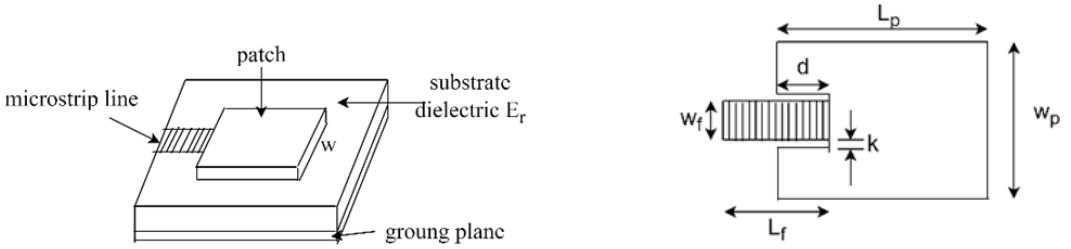

(a) (b)

Figure 2. (a) Patch symbol (b) Geometry of Rectangular Inset_feed patch

2.2 Design formula

The design procedures assume that the specified information includes the dielectric constant of the substrate (εr) and the thickness of the substrate (h), as outlined below:

Specify a center frequency of 5.8 GHz and select a substrate permittivity εr and substrate thickness of 1.6 mm.

$$\mathrm{W} = \frac{1}{2\mathrm{f_r}\sqrt{\mu_0\varepsilon_0}} \times \sqrt{\frac{2}{\varepsilon_\mathrm{r}+1}} \tag{1}$$

For

$$Z_c = \frac{126}{\sqrt{\varepsilon \mathrm{r}}}, {}^{w}/_{h} > 1 \tag{2}$$

$$\varepsilon_{\mathrm{eff}} = \frac{\varepsilon_\mathrm{r}+1}{2} + \frac{\varepsilon_\mathrm{r}-1}{2} \times \left[1 + 12\frac{\mathrm{h}}{\mathrm{w}}\right]^{-0.5} \tag{3}$$

$$\frac{\Delta \mathrm{L}}{\mathrm{h}} = 0.412 \times \left[\frac{(\varepsilon_{\mathrm{reff}}+0.3)\left\{\frac{\mathrm{w}}{\mathrm{h}}+0.264\right\}}{(\varepsilon_{\mathrm{reff}}-0.258)\left\{\frac{\mathrm{w}}{\mathrm{h}}+0.8\right\}}\right] \tag{4}$$

$$\mathrm{L} = \frac{1}{2\mathrm{f_r}\sqrt{\varepsilon_{\mathrm{reff}}}\sqrt{\mu_0\varepsilon_0}} - 2\Delta L \tag{5}$$

For substrate,

$$W_s = 6H + W \tag{6}$$

$$L_s = 6H + L \tag{7}$$

For feed,

$$\mathrm{R_{in}} = \frac{1}{2(\mathrm{G_1}+\mathrm{G_{12}})} \tag{8}$$

$$\mathrm{R_{50\Omega}} = \mathrm{R_{in}}\cos^2\left[\frac{\pi \mathrm{y_0}}{\mathrm{L}}\right] \tag{9}$$

For inset wide (W0) and feed length (L_feed)

$$Z_c = \frac{120\pi}{\sqrt{\varepsilon_\mathrm{r}\left(\frac{\mathrm{w_0}}{\mathrm{h}}1.393+0.667\ln\left(\frac{\mathrm{w_0}}{\mathrm{h}}+1.44\right)\right)}} \tag{10}$$

Calculate the gap of the inset feed, g

$$F = \frac{\mathrm{v_0}}{\sqrt{2\times\varepsilon_{\mathrm{erff}}}} \times \frac{4.6\times10^{-14}}{\mathrm{g}} + \frac{\mathrm{f}}{1.01} \tag{11}$$

Inset feed length, L-feed = $\frac{\lambda}{2}$

The calculated dimensions for the patch in the FEKO simulation are the following:

- Dielectric constant = 4.4
- Height (h) = 1.6 mm
- Velocity of light (c) = 3×10^{8} ms^{-1}
- Practical width (W) = 2.04 mm
- Practical Length (L) L = 1.7407 mm

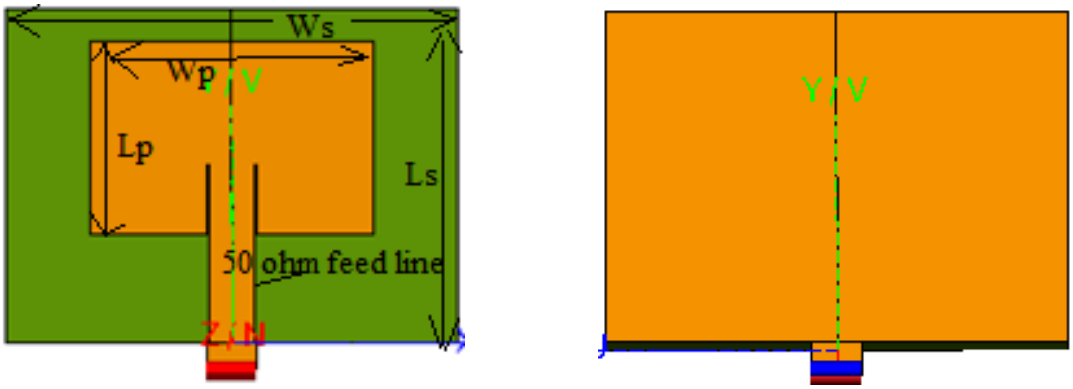

(a) (b)

Figure 3. Single patch antenna (a) top view (b) bottom view

Step 2 is to develop an array using the parameters of the single patch. It uses a corporate feed network adjusted with parametric studies, a microstrip single patch element was organized into 2×1 array to increase antenna performance (Aihsan et al., 2021; Emara et al., 2023; Jeyapoornima & Jeya Sheela, 2024; Olawoye & Kumar, 2022). The rectangular-patch antenna array consists of two rectangular patches and their 50 Ω transmission lines, with the phased center positioned at the array's center. In this design, the matching network is implemented using a microstrip line transmission. The network is symmetrical, as the patches have identical geometry, and it is constructed with a 100 Ω T-patch, two 70.71 Ω quarter wavelength transformers, and a 50 Ω microstrip transmission line (Alkurt et al., 2023; Irfansyah et al., 2021; Rojas et al., 2023). Figure 4 is the basic diagram of the array antenna design. Figure 5 to figure 6 are the graphical method of the research flow.

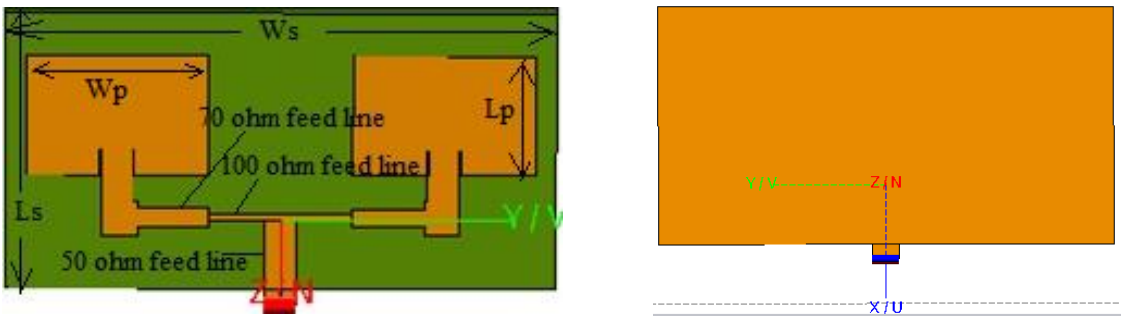

(a) (b)

Figure 4. Basic diagram of antenna array (a) top view (b) bottom view

Table 1 presents the single patch and array parameter dimensions from the calculated results and resonator dimensions.

Table 1. Single patch and array parameter dimensions

Parameters	Single patch antenna	2×1 Array
Dielectric	4.4	4.4
Substrate thick, h	1.6	1.6
Patch width, Wp	17mm 0.328λ_0	17mm 0.328 λ_0
Patch Length, Lp	11.8mm 0.228 λ_0	11.8mm 0.228λ_0
Substrate Width, Ws	26mm 0.5 λ_0	50mm 0.75 λ_0
Substrate Length, Ls	22mm 0.425 λ_0	26mm 0.425 λ_0
Inset_feed position	4.3462mm	4.3462mm
Inset wide, Wf	2.9836	2.9836
Inset_feed length, Lf	6.598	6.598
Gap of the inset_feed	0.086778	0.086778
100 Ω feed line	-	0.55mm
50 Ω feed line	-	1.52mm
70 Ω feed line	-	2.9mm
Ground slots		12× 1.2 mm^2
Resonator (between patches)		11.2× 0.36 mm^2

However, mutual coupling is the major issue of the array antenna, and the separation between the antennas is <λ/2 (Kumar et al., 2021). The restriction on the array, the distance between the centers of the patches must be λ/2>d<λ/4 (Emara et al., 2023). The improvement of the bandwidth is achieved using Defective Ground Structure Method (DGS) (Alkurt et al., 2023; B et al., 2024; En-naghma et al., 2025; Kumar et al., 2021; Natali et al., 2024; Olawoye & Kumar, 2022). An etching approach was slotted, protruding ground stub structure, and parasitic elements/structures (Kumar et al., 2021).

The antenna gain has been improved by incorporating a triangle strip into the ground plane. One horizontal and one vertical slot (DGS) were used and located at the bottom of the patch to improve the bandwidth and gain (Emara et al., 2023). Two defective ground structures in an array, one frame-shaped DGS, and another rectangular-shaped DGS were analyzed (Natali et al., 2024). Additionally, a compact-size array antenna with modified carpet fractal slots with defective ground structure was also studied (Raj & Mandal, 2024). A multitude of hexagonal microstrip patches that is integrated and applied into the defective ground structure method was presented (B et al., 2024). Furthermore, the length and width of the patch ground influences on the return loss were investigated (En-naghma et al., 2025). In step 3, as in Figure 4 (a), is a schematic diagram of an antenna array with added slots and a resonator (0.36 mm × 11.2 mm) between patches. Figure 5 (b) is a schematic diagram of an antenna array with slots added at the ground plane (1.2 mm × 12 mm). Figure 6 shows the positions and dimensions of the slot pairs and resonator.

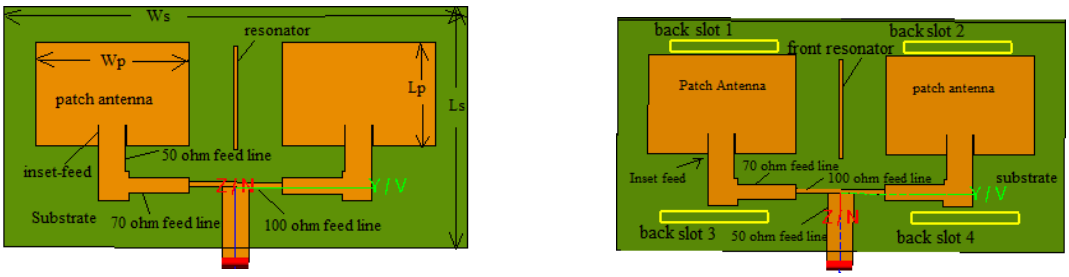

(a) (b)

Figure 5. (a) Schematic diagram of antenna array with added resonator between patches, and (b) Schematic diagram of antenna array with added slots at the ground plane

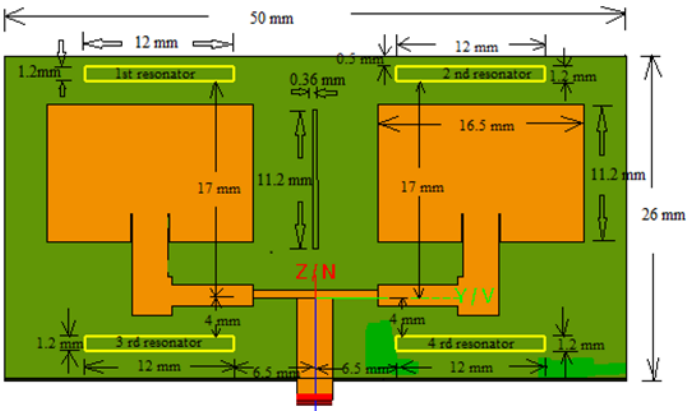

Figure 6. The geometry of position slots and resonator in the array antenna

3. Results and discussion

This section presented the simulated results and discussion for both the array antenna parameters and the resonator array configurations. The design objectives focus on analyzing the insertion of resonator and slots on the patch and ground plane to enhance bandwidth and adjust the resonance frequency. To achieve this, the size and positions of the resonators are carefully analyzed.

Table 2. Positions and sizes of the front side and bottom side resonators

Resonators/ position	Front resonator Size, position (U, V)	Back slot1 Size/position (U, V)	Back slot 2 Size/position (U, V)	Back slot 3 Size/position (U, V)	Back slot 4 Size/ position (U, V)
No resonator	-	-	-	-	-
First position	11.2×0.36, (-4,-0.8)	1.2×12, (-17,-6.5)	1.2×12, (-17,6.5)	1.2×12, (4,-6.5)	1.2×12, (4,6.5)
Second position	11.2×0.36, (-4,-0.8)	1.2×12, (-19,-6.5)	1.2×12, (-19,6.5)	1.2×12, (4,-6.5)	1.2×12, (4,6.5)
Third position	11.2×0.36, (-4,-0.8)	1.2×12, (-17,-7)	1.2×12, (-17,7)	1.2×12, (3.5,-7)	1.2×12, (3.5,7)
Fourth position	11.2×0.36, (-4,-0.8)	1.2×12, (-17,-7)	1.2×12, (-17,7)	1.2×12, (3.5,-8)	1.2×12, (3.5,8)
Fifth position	11.2×0.36, (-4,-0.8)	1.2×12, (-17,-8)	1.2×12, (-17,8)	1.2×12, (3.5,-8)	1.2×12, (3.5,8)
sixth position	11.2×0.36, (-4,-0.8)	1.2×12, (-17,-7)	1.2×12, (-17,7)	1.2×12, (3,-8)	1.2×12, (3,8)
Seventh position	11.2×0.36, (-4,-0.8)	1.2×12, (-17,-7)	1.2×12, (-17,7)	1.2×12, (2.5,-8)	1.2×12, (2.5,8)

Table 2 depicts the positions and sizes of the front resonator and back resonators. The front resonator is placed centre of the array antenna, and the bottom side of the resonators are adjusted. The sizes of the front resonator and back resonator are fixed, while the positions of the back 4 resonators are adjusted. Figure 7 depicts the current direction of the patch antenna at both the front and back positions. The current direction around the front resonator enhances the antenna's bandwidth. The magnetic field of the back resonators can adjust the antenna's resonance frequency and gain.

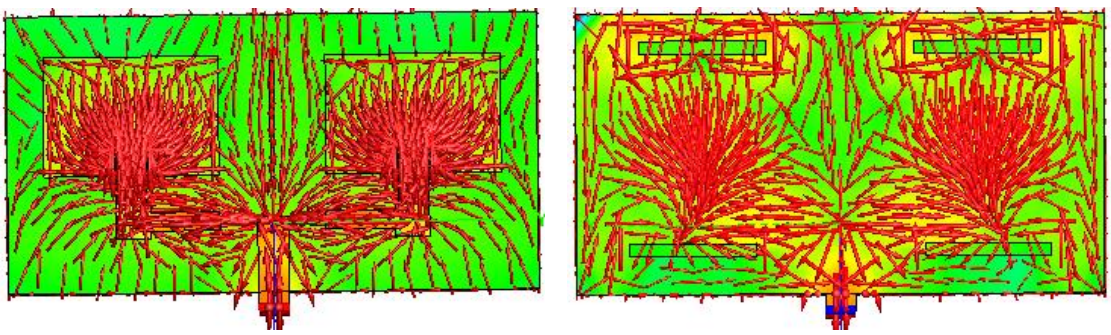

Figure 7. The current direction of the array patch's front side and back side

The simulation results of the antenna array are in the following. Figure 6 shows the current distribution of the patch antenna's front and back sides. Figure 8 illustrates the Reflection coefficient of the array antenna without resonators and the placements of resonators. Figure 9 shows the VSWR of the array antenna without resonators and the placements of resonators.

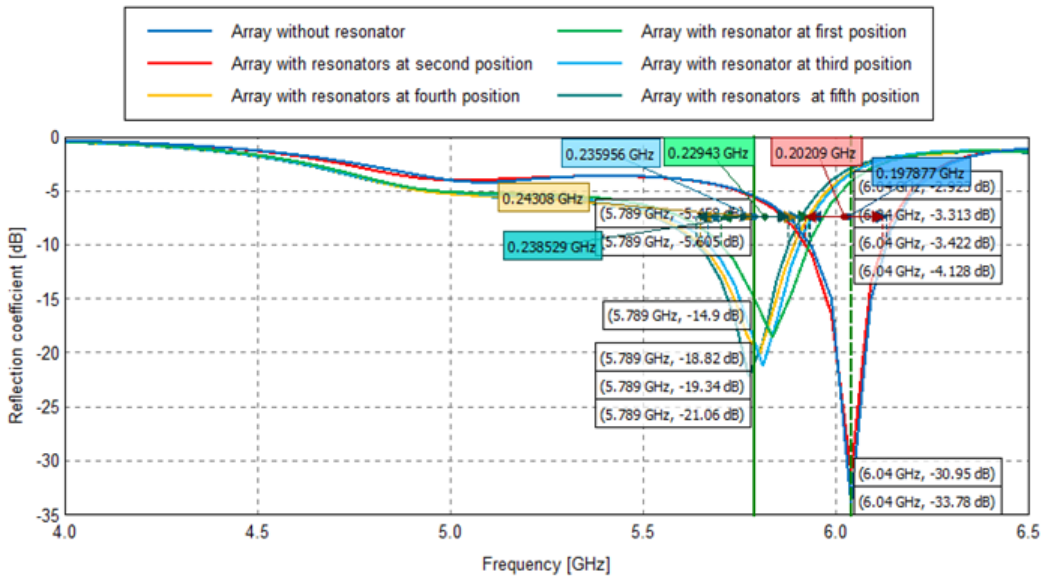

Figure 8. Reflection coefficient of the array antenna without and with resonators based on their placements

Figure 9 is the realized gain of the array antenna without resonators based on their placements. Figures 10 and 11 show the far field of the array without and with resonators at phi = 0 degrees and phi = 90 degrees. Table 3 illustrates the results of the parameters and positions of resonators in the array antenna.

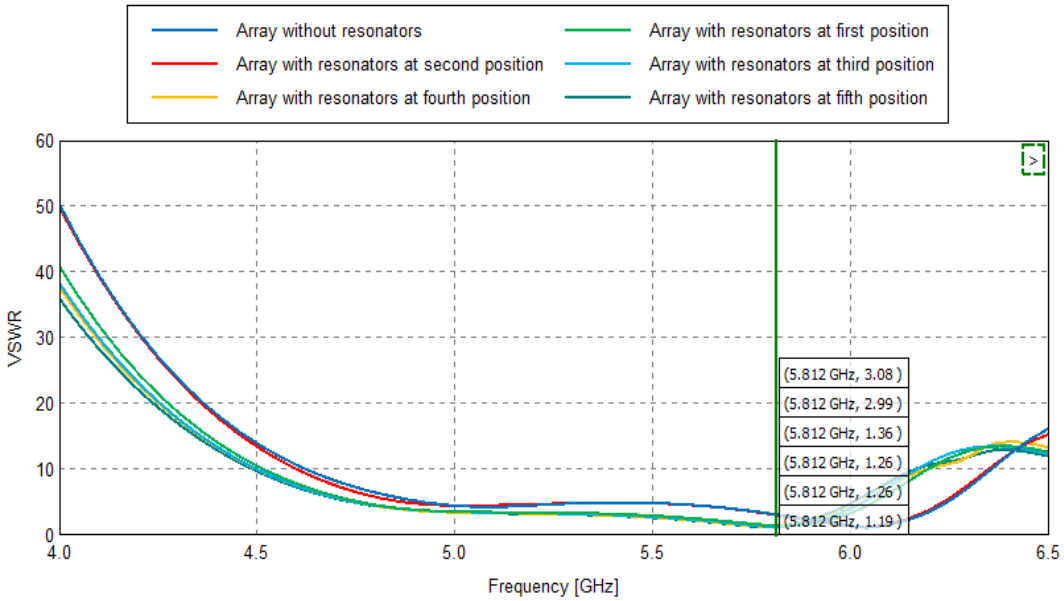

Figure 9. VSWR of array antenna without and with resonators based on their placements

In the first configuration, a rectangular resonator (11.2 × 0.36) mm is positioned at the center of the array. Four slotted resonators are placed on the bottom side, with a dimension of 12 mm × 1.2 mm, located 6.5 mm from the center along the x direction. The upper resonators are 17 mm from the reference center, and the bottom resonators are placed 4 mm from the reference center along the y-direction. This configuration results in a resonance frequency of 5.84 GHz,

a reflection coefficient of -18.9 dB, an increased bandwidth of 238 MHz, a VSWR of 1.28, and a realized gain of 7.26 dBi.

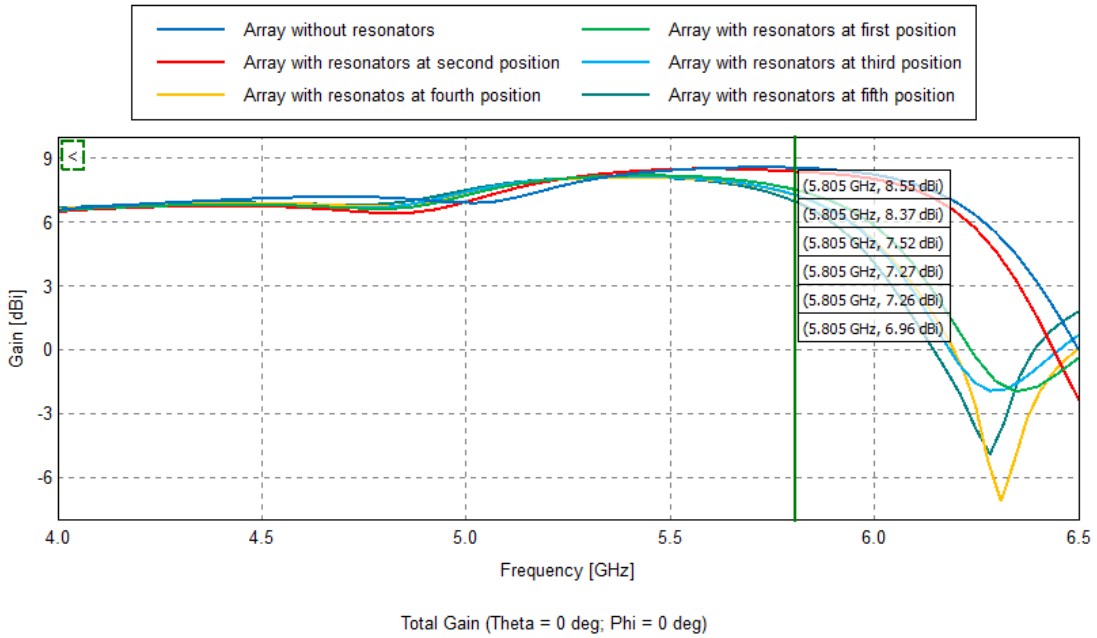

Figure 10. Realized gain of the array antenna without and with resonators based on their placements

In the second configuration, the resonators in the x-direction remain unchanged, while in the y-direction, the upper resonator is moved to 17 mm from the reference center. In the second position, the resonance frequency becomes 6.04 GHz, the reflection coefficient is -25.12 dB, the bandwidth is 204 MHz, VSWR is 1.13 and the realized gain becomes 7.89 dBi. In the third configuration, the bottom resonators in the y direction are moving 3.5 mm (instead of 4mm), while all resonators in the x direction are shifted 7 mm from the reference center, replacing the previous 6.5 mm position. This results in a resonance frequency become 5.8 GHz, a reflection coefficient is -21.18 dB, a bandwidth is 234 MHz, a VSWR is 1.19 and a realized gain become 7.2 dBi.

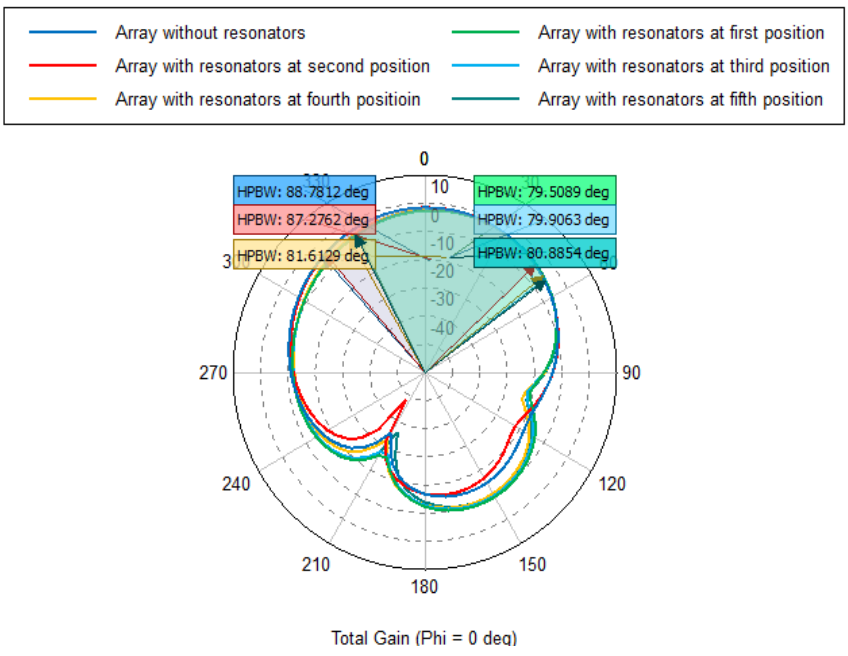

Figure 11. Fairfield of array with and without resonators at phi = 0 degrees

In the fourth configuration, the y-direction remains unchanged, but the two bottom side resonators in the x-direction are shifted to 8 mm from the center, compared to the 7 mm. This configuration yields a resonance frequency of 5.8 GHz, a reflection coefficient of -19.89 dB, a bandwidth is 243 MHz, a VSWR of 1.2, and a realized gain of 7.21 dBi. For the fifth configuration, the bottom resonators in the y direction are unchanged, while in the x direction, the shifted upper resonators are 8mm. In this position, the resonance frequency becomes 5.82 GHz, the reflection coefficient is -20.9 dB, the bandwidth is 242 MHz, the VSWR is 1.2, and the realized gain becomes 7.41 dBi.

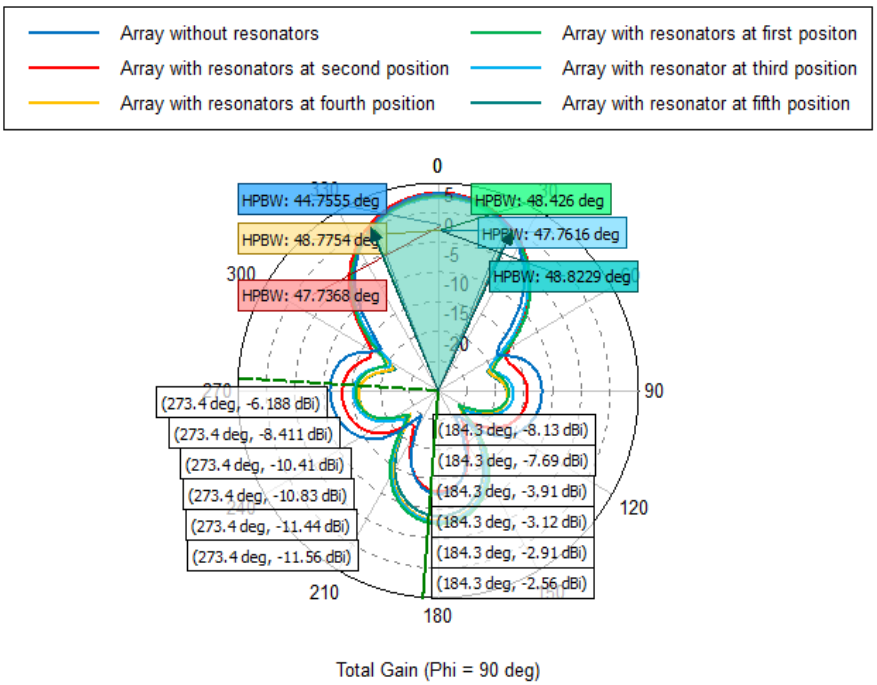

Figure 12. Fairfield of the array with and without resonators at phi = 90 degrees

For the sixth configuration, the bottom resonators in the y direction are moved 3 mm (instead of 3.5 mm), with the x direction remaining unchanged. In this position, the resonance frequency becomes 5.78 GHz, the reflection coefficient is -29.14 dB, the bandwidth is 238 MHz, the VSWR is 1.18, and the realized gain becomes 7.08 dBi. Finally, in the seventh configuration, the bottom resonators in the y direction are moved 2.5 mm (instead of 3 mm), with the x direction remaining unchanged. The result is a resonance frequency of 5.75 GHz, a reflection coefficient of -20.62 dB, a bandwidth of 233 MHz, a VSWR of 1.21, and a realized gain of 6.9 dBi.

Table 3. Results of parameters and positions of resonators in the array antenna

Results/ position	Resonance frequency	Reflection coefficient	Bandwidth	VSWR	Realized gain
Single patch	5.66 GHz	-12.3 dB	0.184 GHz	1.64	5.75 dBi
Basic 2×1 array	6.04 GHz	-33.7 dB	0.198 GHz	1.3	8.21 dBi
First position	5.836 GHz	-18.9 dB	0.238 GHz	1.28	7.26 dBi
Second position	6.04 GHz	-25.1 dB	0.204 GHz	1.13	7.89 dBi
Third position	5.81 GHz	-21.2 dB	0.234 GHz	1.19	7.2 dBi
Fourth position	5.8 GHz	-19.9 dB	0.243 GHz	1.2	7.21 dBi
Fifth position	5.82 Ghz	-20.9 dB	0.242 GHz	1.2	7.41 dBi
Sixth position	5.78Ghz	-29.1 dB	0.238 GHz	1.18	7.08 dBi
seventh position	5.75 GHz	-20.6 dB	0.233 GHz	1.21	6.9 dBi

Table 4 is a comparison of the proposed work and the references. The frame shape defective ground structure has more bandwidth than the rectangular shape defective ground structure (Natali et al., 2024). The result indicated that the fractal slots with a DGS array structure antenna have a large bandwidth and good impedance matching with a -41.83 dB (Raj & Mandal, 2024). In comparison, the proposed array antenna configurations (slotted with a ground plane) harvest the highest gain of 7.42 dBi with a suitable bandwidth of 243 MHz and good impedance matching of VSWR 1.2. The band difference between without a slotted ground and with a slotted ground is about 0.05 GHz. The antenna size is minimized and gain also highest compared with all 2×1 reference antenna design. The results are enough for detecting respiratory rate of the human body.

4. Conclusion

In conclusion, the analysis of rectangular slot patch placement and dimensions suggests that symmetrical placement is more suitable for enhancing antenna performance. Enhancing the bandwidth and gain of the antenna improves its performance, allowing for more detailed data acquisition of the human body's respiratory rate. Moreover, the contribution of enhancing antenna performance by adding rectangular slots to the ground or DGS is attractive for energy-harvesting wireless transmission technologies and biomedical applications. This work focuses on detecting contactless respiratory rate of stationary human positions, while future work will involve detecting moving body using circular polarization.

Author's Declaration

Author contribution

Cing Nuam Man: Conceptualization, Software, Investigation, and Writing - Original Draft. **Thanda Win**: Validation, Formal analysis and Data Curation. **Hla Myo Tun**: Conceptualization, Supervision, Validation, and Writing - Review & Editing. **Mya Mya Aye**: Supervision, Validation, and Writing - Review & Editing.

Funding statement

This research received no specific grant from any funding agency in the public, commercial, or not-for-profit sectors.

Acknowledgement

The authors would like to thank those who have helped in the implementation of this research.

Competing interest

The authors declare no conflict of interest from the conduct of research and publication of this article.

Ethical Clearance

This research does not involve humans or animals as subjects.

AI Statement

This article is an original work of the authors without including any AI generated sentences, tables, and images. The grammatical structure of this article was improved by using ChatGPT and the authors have rechecked the accuracy, correctness, and suitability with the topic and data of this study. The language use in this article has been validated and verified by an English language expert.

Publisher's and Journal's Note

Researcher and Lecturer Society as the publisher, and the Editor of Journal of Engineering Researcher and Lecturer state that there is no conflict of interest towards this article publication.

References

Aihsan, M. Z., Hariz, M. F., Mustafa, W. A., Idrus, S. Z. S., Rahim, H. A., & Alkhayyat, A. (2021). Design and Simulation of 2×1 and 2×2 Array Antenna at 5.8 GHz for Gain and Axial Ratio Enhancement. *2021 International Conference on Advanced Computer Applications (ACA)*, 223–227. https://doi.org/10.1109/ACA52198.2021.9626803

Alkurt, F. O., Unal, E., Palandoken, M., Abdulkarim, Y. I., Hasar, U. C., & Karaaslan, M. (2023). Radiation pattern reconfigurable cubical antenna array for 2.45 GHz wireless communication applications. *Wireless Networks*, *29*(1), 235–246. https://doi.org/10.1007/s11276-022-03116-4

B, U. R., Koteswara Rao, N. V, & Sekhar, P. C. (2024). Design of Integrated Hexagonal Microstrip Patch Antenna with DGS for Wideband Applications. *2024 IEEE Wireless Antenna and Microwave Symposium (WAMS)*, 1–5. https://doi.org/10.1109/WAMS59642.2024.10527915

Balanis, C. A. (2009). Antenna Theory: Analysis and Design, (3RD ED.). In *Wiley India Pvt. Limited*.

Emara, H. M., El Dyasti, S. K., Ghouz, H. H. M., Fathy Abo Sree, M., & Abdel Fatah, S. Y. (2023). Compact High Gain Microstrip Array Antenna Using DGS Structure for 5G Applications. *Progress In Electromagnetics Research C*, *130*, 213–225. https://doi.org/10.2528/PIERC22122110

En-naghma, W., Latrach, M., Halaq, H., & El Ougli, A. (2025). An experimental study of a high-gain, wideband circularly polarized printed antenna array at 2.45 GHz in the ISM band for wireless power transmission applications. *Scientific African*, *27*, e02619. https://doi.org/10.1016/j.sciaf.2025.e02619

Hamad, E. K. I., & Abdelaziz, A. (2019). Performance of a Metamaterial-based 1×2 Microstrip Patch Antenna Array for Wireless Communications Examined by Characteristic Mode Analysis. *Radioengineering*, *28*(4), 680–688. https://doi.org/10.13164/re.2019.0680

Irfansyah, A., Harianto, B. B., & Pambudiyatno, N. (2021). Design of Rectangular Microstrip Antenna 1x2 Array for 5G Communication. *Journal of Physics: Conference Series*, *2117*(1), 012028. https://doi.org/10.1088/1742-6596/2117/1/012028

Jeyapoornima, B., & Jeya Sheela, J. J. (2024). Design of Antenna Array of 2x1 Configuration for Microwave Imaging. *2024 IEEE International Conference on Communication, Computing and Signal Processing (IICCCS)*, 1–5. https://doi.org/10.1109/IICCCS61609.2024.10763824

Kadir Al-Nahiun, S. A., Mahbub, F., Islam, R., Akash, S. B., Hasan, R. R., & Rahman, Md. A. (2021). Performance Analysis of Microstrip Patch Antenna for the Diagnosis of Brain Cancer & Tumor using the Fifth-Generation Frequency Band. *2021 IEEE International IOT, Electronics and Mechatronics Conference (IEMTRONICS)*, 1–6. https://doi.org/10.1109/IEMTRONICS52119.2021.9422503

Kumar, A., Ansari, A. Q., Kanaujia, B. K., Kishor, J., & Matekovits, L. (2021). A Review on Different Techniques of Mutual Coupling Reduction Between Elements of Any MIMO Antenna. Part 1: DGSs and Parasitic Structures. *Radio Science*, *56*(3). https://doi.org/10.1029/2020RS007122

Lakrit, S., Ammor, H., Matah, S., Karli, R., Saadi, A., Terhzaz, J., & Tribak, A. (2018). A new small high-gain wideband rectangular patch antenna for X and Ku bands applications. *Journal of Taibah University for Science*, *12*(2), 202–207. https://doi.org/10.1080/16583655.2018.1451105

Liu, X., Di, Y., Liu, H., Wu, Z., & Tentzeris, M. M. (2016). A Planar Windmill-Like Broadband Antenna Equipped With Artificial Magnetic Conductor for Off-Body Communications. *IEEE Antennas and Wireless Propagation Letters*, *15*, 64–67. https://doi.org/10.1109/LAWP.2015.2429683

Natali, Y., Irvana, R., Yudiansyah, Y., Widi Astuti, D., Astuti C, D., & Apriono, C. (2024). Study on Defected Ground Structure Models with Miniaturized Patches for Broadband Wireless Systems. *Journal of Communications*, 168–174. https://doi.org/10.12720/jcm.19.3.168-174

Olawoye, T. O., & Kumar, P. (2022). A High Gain Antenna with DGS for Sub-6 GHz 5G Communications. *Advanced Electromagnetics*, *11*(1), 41–50. https://doi.org/10.7716/aem.v11i1.1670

Pepe, D., Vallozzi, L., Rogier, H., & Zito, D. (2013). Planar Differential Antenna for Short-Range UWB Pulse Radar Sensor. *IEEE Antennas and Wireless Propagation Letters*, *12*, 1527–1530. https://doi.org/10.1109/LAWP.2013.2291957

Poffelie, L. A. Y., Soh, P. J., Yan, S., & Vandenbosch, G. A. E. (2016). A High-Fidelity All-Textile UWB Antenna With Low Back Radiation for Off-Body WBAN Applications. *IEEE Transactions on Antennas and Propagation*, *64*(2), 757–760. https://doi.org/10.1109/TAP.2015.2510035

Raj, A., & Mandal, D. (2024). Design and performance analysis of fractal slot array antenna for advanced 5G mm-wave applications. *International Journal of Electronics*, 1–23. https://doi.org/10.1080/00207217.2024.2408788

Rojas, J. M., Reyes-Ayala, M., Andrade-Gonzalez, E. A., Chavez-Sanchez, S., Terres-Peña, H., & Rodriguez-Rivera, R. (2023). 2 x 1 Rectangular-Patch Antenna Array at 2.4 GHz. *Wseas Transactions on Communications*, *22*, 49–57. https://doi.org/10.37394/23204.2023.22.5

Yang, Z., Bocca, M., Jain, V., & Mohapatra, P. (2018). Contactless Breathing Rate Monitoring in Vehicle Using UWB Radar. *Proceedings of the 7th International Workshop on Real-World Embedded Wireless Systems and Networks*, 13–18. https://doi.org/10.1145/3277883.3277884

Yousaf, M., Mabrouk, I. Ben, Zada, M., Akram, A., Amin, Y., Nedil, M., & Yoo, H. (2021). An Ultra-Miniaturized Antenna With Ultra-Wide Bandwidth Characteristics for Medical Implant Systems. *IEEE Access*, *9*, 40086–40097. https://doi.org/10.1109/ACCESS.2021.3064307

Zito, D., & Pepe, D. (2014). Planar Differential Antenna Design and Integration With Pulse Radar Microchip Sensor. *IEEE Sensors Journal*, *14*(8), 2477–2487. https://doi.org/10.1109/JSEN.2013.2295678